Pergamon

0022-3697(95)00041-0

J. Phys. Chem. Solids Vol. 56, No. 7, pp. 995–1001, 1995

0022-3697/95 $9.50 + 0.00

LOCAL STRUCTURE DETERMINATION OF Mn^{2+} IN THE $ABCl_3:Mn^{2+}$ CHLOROPEROVSKITES BY EXAFS AND OPTICAL SPECTROSCOPY

M. C. MARCO DE LUCAS,[a] F. RODRÍGUEZ,[a]† C. PRIETO,[b] M. VERDAGUER[c,d] and H. U. GÜDEL[e]

[a]D.C.T.T.Y.M. Facultad de Ciencias, Universidad de Cantabria, 39005 Santander, Spain
[b]Instituto de Ciencias de Materiales (C.S.I.C.) Facultad de Ciencias (CIV), Cantoblanco, 28049 Madrid, Spain
[c]Laboratoire de Chimie des Metaux de Transition, Université Pierre et Marie Curie, 75252 Paris, Cedex 05, France
[d]L.U.R.E., Université Paris-Sud, 91405 Orsay Cedex, France
[e]Institut für Anorganische Chemie der Universität Bern, Freiestrasse 3, CH-3000, Bern 9, Switzerland

(*Received* 10 *October* 1994; *accepted* 13 *January* 1995)

Abstract—This work reports the local structure around the manganese in the $ABCl_3:Mn^{2+}$ (A = K, Rb, Cs and B = Mg, Ca, Cd, Sr) chloroperovskite series. EXAFS and XANES experiments carried out in $KMgCl_3:Mn^{2+}$ and $RbCaCl_3:Mn^{2+}$ indicate that the Mn–Cl distances of the $MnCl_6^{4-}$ complex are 2.51 and 2.53 Å, respectively. These values are very similar to those found in the pure NH_4MnCl_3 perovskite, $R = 2.525$ Å, and show that the variations of R along the series do not follow that of the host lattice. The correlation between these measurements and the optical excitation spectra allows us to estimate Mn–Cl bond distances for the whole series with accuracies of about 0.002 Å. The present results are compared with previous structural data reported for the $ABF_3:Mn^{2+}$ isomorphous fluorides.

Keywords: XAFS (EXAFS and XANES) (C) Crystal fields (D) Luminescence (D) Optical properties (D) inorganic compounds (A).

1. INTRODUCTION

Some transition metal impurities play a fundamental role in the physical properties of inorganic compounds. A proper microscopic understanding of such properties requires a knowledge of the local structure around the impurity; that is the neighborhood ions, site symmetry and bond distances. In wide band gap insulating crystals, the complex formed by the impurity ion and its nearest neighbors can usually account for the properties. Apart from the ligands and their coordination polyhedra which can be revealed by standard selective techniques such as EPR, Raman scattering or optical spectroscopy, the determination of bond distances is still a difficult task for many doped materials in spite of the continuous improvements in EXAFS techniques in the last few years. In particular, this technique has serious limitations for impurity concentrations below 1 mol%, as well as for determining metal–ligand distances with accuracies better than 0.02 Å. Due to this fact, the accurate structural characterization of impurities is presently known only for a very small number of systems. Technologically important crystals such as Al_2O_3 doped with Ti or Cr and perovskites ABX_3 or elpasolites A_2BMX_6 (X = F, Cl) doped with Cr, Mn, Cu, etc., are clear examples of this lack of information about the immediate environment of the optical center.

Local structure determinations by EXAFS have been performed for CaF_2 doped with trivalent rare earth ions [1, 2], Mn^{2+} [3] in $RbCdF_3:Mn^{2+}$ and $KZnF_3:Mn^{2+}$ [4] but for crystals with impurity concentrations greater than 1 mol%. Interestingly, the EXAFS measurements carried out on perovskite oxides such as $KTaO_3$: Nb [5] and $LiNbO_3$: Ni, Ti [6] proved to be useful for investigating the nature of the different centers formed, as well as to clarify the atomic displacements of the impurity across the ferroelectric phase transition.

Nevertheless, these experimental limitations can be largely overcome using EXAFS in connection with complementary techniques which are sensitive to both low impurity concentrations and small variations of the interatomic distances. Suitable procedures based on the variation of the isotropic superhyperfine constant, A_S, [7] and the ligand field parameter, $10Dq$, [8, 9] with the impurity–ligand

† Author for correspondence.

distance, R, have been developed by Moreno *et al.* for determining bond distances in the Mn^{2+} doped ABF_3 fluoroperovskite series. A salient conclusion of that work is that R corresponds neither to the cation–F distance of the host lattice nor the sum of F^- and Mn^{2+} ionic radii, but instead the actual R value is given by the equation $\Delta R = R - R_{Mn\text{-}F} = 0.30\,(a_0/2 - R_{Mn\text{-}F})$, where R is the actual Mn–F distance, $R_{Mn\text{-}F} = 2.13$ Å is the sum of ionic radii, and a_0 is the cubic host lattice parameter. Thus this result shows that either an inward or an outward relaxation of the F ligands around the Mn^{2+} occurs whenever $a_0/2$ is greater or smaller than 2.13 Å, respectively.

The aim of the present work is to investigate by means of EXAFS and optical spectroscopy techniques the local structure around the Mn^{2+} in the series of chloroperovskites $KMgCl_3$, $KCaCl_3$, $RbCaCl_3$, $RbCdCl_3$, $CsCaCl_3$, $RbSrCl_3$ and $CsSrCl_3$ doped with Mn^{2+}. The interest in this series lies in extending the study of the fluoperovskite series to the nearly isomorphous $ABCl_3$ crystals, replacing F^- by the more covalent Cl^- anion. The effect of the host crystal upon the impurity–ligand distance is studied as a function of the molecular cell volume. It must be noted that most of the $ABCl_3$ crystals have the cubic Pm3m perovskite structure above room temperature (Table 1), but at lower temperatures, all crystals undergo a structural phase transition sequence which is mainly associated with the condensation of the R_{25} and M_3 phonon modes. Structurally, these transitions mainly involve rotations of the BCl_6 inorganic octahedra around different crytallographic directions [10, 11]. The non-displacive character of these transitions in both chlorides and fluorides allows the BX_6 units to keep a nearly octahedral symmetry with similar B–X distances. A good example of this behavior is $KMgCl_3$ with Mg–Cl distances in the room temperature orthorhombic Pnma structure of 2.501, 2.496 and 2.502 Å [12].

It should also be noted that EXAFS measurements are more difficult to make in transition metal doped chlorides than in the corresponding fluorides, due to the higher absorption coefficient of the Cl^- ion. In particular, the manganese K-edge contribution to the background absorption coefficient ratio, $\Delta\mu/\mu$, is about 0.03 and 0.015 in the most favorable case of $KMgF_3$ and $KMgCl_3$ doped with 2 mol% of Mn^{2+}, respectively [13]. In addition, difficulties also arise because the variation of the Mn–Cl distance along the $ABCl_3:Mn^{2+}$ series is expected to be much smaller than that observed for the corresponding $ABF_3:Mn^{2+}$ series due to the higher compressibilities of the chloride lattices.

Suitable EXAFS spectra could be obtained for $KMgCl_3:Mn^{2+}$, $KCaCl_3:Mn^{2+}$ and $RbCaCl_3:Mn^{2+}$ working in the X-ray fluorescence mode instead of the standard absorption mode, which could not be used for the present $ABCl_3:Mn^{2+}$ crystals. Furthermore, the structural study has been correlated with the optical excitation spectra which are a very sensitive probe of variations in R. In fact, some of the Mn^{2+} bands are strongly dependent upon the ligand field parameter, $10Dq$, which usually has an R^{-n} dependence with n close to 5. Therefore variations of R down to $2 \cdot 10^{-3}$ Å can be detected by this technique provided that $10Dq$ variations of 20 cm^{-1} can be measured.

2. EXPERIMENTAL

Single crystals of $KMgCl_3$, $KCaCl_3$, $RbCaCl_3$, $RbCdCl_3$, $CsCaCl_3$, $RbSrCl_3$ and $CsSrCl_3$ doped with 1 mol% of Mn^{2+} were grown by the Bridgman technique [12]. This low concentration is employed in order to prevent dimer formation, which occurs above 10%. The room temperature excitation spectra in the 300–600 nm range were obtained as described elsewhere [12]. The spectra were not corrected for instrumental response.

All the EXAFS spectra were measured at room temperature at the Mn K edge ($E_0 = 6550$ eV) using the excitation mode setup at the XAS-3 (DCI) station at LURE, which is equipped with a double crystal Si (311) monochromator. The beam energy was 1.85 GeV with a maximum stored intensity of 300 mA. Spectra were recorded using stepsizes of 2 eV (EXAFS) and 0.3 eV (XANES) in the 6450–7450 eV excitation range by detection of the whole X-ray fluorescence with counting times of 2 s per step. Five runs were averaged for each spectrum. In order to minimize the excitation beam and Bragg reflections, a 0.1 mm chromium filter was placed between sample and detector. In addition, the crystals were ground under paraffin because some compounds are extremely hygroscopic. In spite of this precaution, hydration and decomposition of the $RbSrCl_3$ crystal could not be avoided. Traces of RbCl and $SrCl_2 \cdot 6H_2O$ were clearly identified in the corresponding X-ray diffraction diagram.

EXAFS oscillations were observed for Mn^{2+} doped $KMgCl_3$, $KCaCl_3$ and $RbCaCl_3$, but the spectrum of the $KCaCl_3$ was so noisy that no reliable structural data could be extracted. For the remaining crystals, the Mn signal was completely masked by the intense X-ray fluorescence of the Cs and Cd ions.

Spectra were analysed with the software program package developed by A. Michalowitz [15, 16]. Due to low Mn concentration, only three EXAFS oscillations were clearly detected in $KMgCl_3$ and $RbCaCl_3$, and thus structural information beyond the

Table 1. Space group, lattice parameters (Å), cubic phase transition temperature, T_C(K), host distance, R_L (see eqn (3)), Mn^{2+} ligand field parameter, $10Dq$, and the corresponding Mn–Cl distance, R, obtained from eqn (2), for the $ABCl_3:Mn^{2+}$ crystal series. Estimated errors for $10Dq$ and R are 20 cm^{-1} and 0.002 Å, respectively

System	Crystal structure and lattice parameters (Å) at room temperature	Pm3m transition temperature T_C (K)	Host distance R_L (Å)	$10Dq$ (cm^{-1})	Mn–Cl distance R (Å)
$KMgCl_3:Mn^{2+}$	Orth. Pnma [25] $a = 6.967$ $b = 9.917$ $c = 6.967$ $Z = 4$	569 [26]	2.47	5768	2.512
$RbCdCl_3:Mn^{2+}$	Orth. Pnam [27] $a = 8.959$ $b = 14.967$ $c = 4.035$ $Z = 4$	388 [28]	2.56	5622	2.525
$KCaCl_3:Mn^{2+}$	Orth. Pnma [12, 29] $a = 7.561$ $b = 10.480$ $c = 7.255$ $Z = 4$	909 [29, 30]	2.61	5434	2.542
$RbCaCl_3:Mn^{2+}$	Orth. Pnma [27] $a = 7.541$ $b = 10.667$ $c = 7.469$ $Z = 4$	573 [30]	2.66	5442	2.541
$CsCaCl_3:Mn^{2+}$	Cub. Pm3m [11, 27] $a = 5.382$ $Z = 1$	95 [11]	2.69	5375	2.548
$CsSrCl_3:Mn^{2+}$	Orth. Pnma [31] $a = 7.92$ $b = 11.25$ $c = 7.92$ $Z = 4$	385 [32, 33]	2.80	5196	2.565
$RbSrCl_3:Mn^{2+}$	Mon. $P2_1/m$ [31] $a = 7.93$ $b = 11.02$ $c = 7.67$ $\beta = 90.1$ $Z = 4$	629 [31]	2.75	5052	2.579
NH_4MnCl_3 [ ]	Cub. Pm3m [19] $a = 5.050$ $Z = 1$	258 [19]	2.525	5620	2.525

first coordination sphere becomes extremely difficult. Therefore our analysis is limited to the nearest neighbors and focused on determining the Mn–Cl distance in the $MnCl_6^{4-}$ complex formed.

The normalized EXAFS signal, $\chi(E) = (\mu(E) - \mu_0(E))/\mu_0(E)$, was extracted from the experimental data by subtracting the extrapolated pre-edge background from the total excitation signal to obtain $\mu(E)$. The smooth Mn absorption after the Mn K-edge, $\mu_0(E)$, was obtained by fitting the experimental curve to a polynomial of order 5. The EXAFS signal was transformed into k-space, $\chi(k)$, by $k = [2m(E - E_0)]^{1/2}/\hbar$ with $E_0 = 6550.0$ eV. Since we restrict our fitting to the first Cl shell, the weighted $k \cdot \chi(k)$ functions are Fourier transformed using a Hamming window in the 3.28–8.76 $Å^{-1}$ range and then filtered in R-space (1.8–2.3 Å) in order to select the first shell oscillations in the inverse transformed function. It must be emphasized that the *same windows* in k- and R-space have been employed for all spectra. The resulting experimental functions are fitted to the classical expression [17]:

$$\chi(k) = S_0^2 \sum_i \left[N_i A_i(k) \exp(-2\sigma_i^2 k^2) \times \exp\left(-\frac{2R_i}{\lambda(k)}\right) \frac{\sin(2kR_i + \Phi_{ij}(k))}{kR_i^2} \right]. \quad (1)$$

We used $i = 1$ and $N_1 = 6$, and the phase, $\Phi_1(k)$, and amplitude, $A_1(k)$, functions were calculated with the McKale program [15]. The fitting parameters were the Debye–Waller factor, σ_1, the electron mean free path, approximated by $\lambda(k) = [(k + (\eta/k)^4]/\Gamma$, and the Mn–Cl distance, R. Values of $\eta = 3.1$, $\Gamma = 1.115$ and $\sigma_1 = 0.105$ obtained by fitting data from a standard $[(CH_3)_4N]MnCl_3$ (TMMC) crystal ($R = 2.560$ Å) [18], were used as starting parameters for the $ABCl_3:Mn^{2+}$ series. The $\eta = 3.1$ and $\Delta E_0 = 2.1$ eV parameters obtained from the TMMC fit were fixed for the other samples. Apart from R, the only variable parameters over the series were Γ and

σ_1, since this is the minimum number of variable parameters required to account for the slight variations undergone by the Debye–Waller factor and the electron mean free path with the host crystal.

The optical absorption spectrum of the NH_4MnCl_3 perovskite ($R = 2.525$ Å) [19] was employed as a standard for the optical excitation spectra.

3. RESULTS AND DISCUSSION

Figure 1 depicts the room temperature X-ray excitation spectra of the $KMgCl_3:Mn^{2+}$, $KCaCl_3:Mn^{2+}$, $RbCaCl_3:Mn^{2+}$ and the standard TMMC crystals. The spectra show an abrupt peak at $E_0 = 6550.0$ eV, which is associated with the manganese K-edge, followed by the usual EXAFS oscillations containing the local structure information. The corresponding XANES spectra, shown in the inset to Fig. 1, are similar for all the crystals. Their structure resembles that observed for other $MnCl_6^{4-}$ complexes [20] and confirms the octahedral coordination of the Mn^{2+}, already revealed by optical excitation spectroscopy [14]. In fact, the pre-edge features associated with electronic transitions from inner 1s electrons to the 3d ($t + e$ in T_d) orbitals observed in tetrahedrally coordinated $MnCl_4^{2-}$ [20] complexes, are absent in the present compounds as expected for nearly centrosymmetric $MnCl_6^{4-}$ complexes, where these transitions are forbidden by the electric dipole mechanism.

Figure 2 shows the filtered experimental EXAFS signal together with the calculated one from eqn (1). The fitting parameters, Γ, σ_1 and R, are collected in Table 2. Note that the Mn–Cl distance for TMMC given in Table 2 is shifted by 0.01 Å from that obtained by X-ray diffraction techniques [18]. However, it is important to realize that although the absolute R values are determined with an error of 0.02 Å, the variation ΔR along the measured series of crystals is probably more accurate since all the spectra have been analysed under identical conditions.

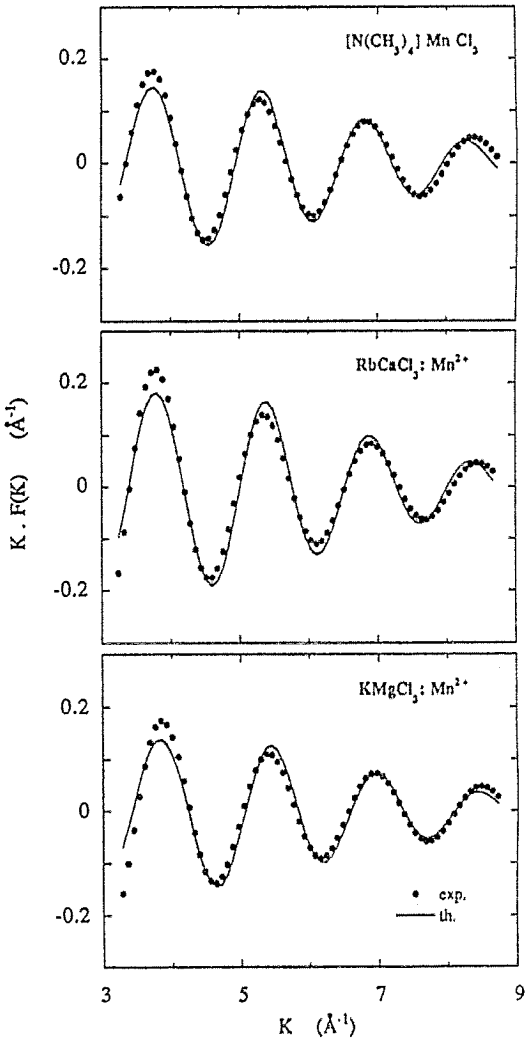

Fig. 2. Filtered experimental signals (points) showing the EXAFS oscillations and the calculated values from fits to eqn (1) (full curves). The fitting parameters are given in Table 2.

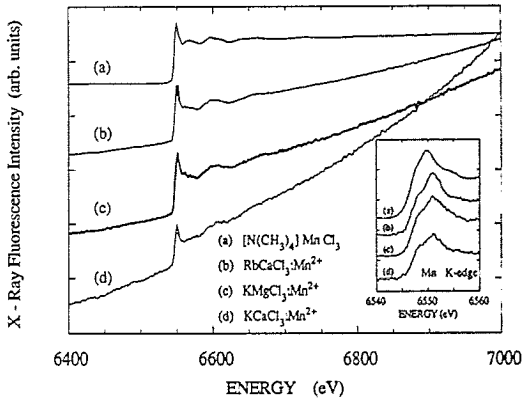

Fig. 1. EXAFS spectra recorded in fluorescence mode for $KMgCl_3:Mn^{2+}$, $RbCaCl_3:Mn^{2+}$, $KCaCl_3:Mn^{2+}$ and the TMMC standard at room temperature. The intensity scale of each spectrum has been properly modified for comparison purposes. The inset shows the corresponding XANES spectra.

The measured R values are considerably shorter than the Mn–Cl distance for the TMMC model compound: $R = 2.560$ Å. This fact may be associated with the more closely packed structure displayed by the perovskite in comparison to one- or two-dimensional structures where Mn–Cl distances become larger with a decrease in the crystal dimensionality, i.e. the reduction of the number of shared $MnCl_6^{4-}$ units. The present 1-D TMMC, the 2-D $[NH_3(CH_2)_2NH_3]MnCl_4$ and the 3-D NH_4MnCl_3 crystals with $R = 2.56$, 2.55 (2.58 (in-plane) + 2.50 (out of plane)) [21] and 2.525 Å, respectively, are examples of this behavior. On the other hand, the difference between the R values obtained for

Table 2. Fitting parameters of the EXAFS spectra to eqn (1) for $KMgCl_3:Mn^{2+}$, $RbCaCl_3:Mn^{2+}$ and the TMMC standard. The estimated EXAFS accuracy is 0.02 Å. The units are given according to eqn (1) using R in Å, k in $Å^{-1}$ and E in eV

System	N	η	ΔE_0	Γ	σ	R
TMMC	6	3.1	2.1	1.11	0.105	2.55 (2)
$KMgCl_3:Mn^{2+}$	6	3.1	2.1	1.12	0.108	2.51 (2)
$RbCaCl_3:Mn^{2+}$	6	3.1	2.1	1.01	0.102	2.53 (2)

$KMgCl_3:Mn^{2+}$ and $RbCaCl_3:Mn^{2+}$, $\Delta R = 0.02$ Å, does not reflect a reduction of the host distance, R_L, on passing from $KMgCl_3$ ($R_L = 2.47$ Å) to $RbCaCl_3$ ($R_L = 2.66$ Å) (Table 1). This result reflects the *molecular character* of the $MnCl_6^{4-}$ units whose equilibrium bond distances are closer to those of the pure NH_4MnCl_3 perovskite than to R_L. In the present case, the influence of the host lattice upon the equilibrium distance is much smaller than for MnF_6^{4-} over the $ABF_3:Mn^{2+}$ series [22].

The present results are also confirmed by the room temperature optical excitation spectra shown in Fig. 3 for $KMgCl_3:Mn^{2+}$, $KCaCl_3:Mn^{2+}$ and $CsSrCl_3:Mn^{2+}$. A complete analysis of the spectra of the whole series is given elsewhere [14]. The observed bands and the corresponding transition energies clearly indicate that Mn^{2+} is placed at the divalent cation site, forming octahedral $MnCl_6^{4-}$ units. The corresponding $10Dq$ values derived from such spectra are also included in Table 1.

The sensitivity of these spectra to detect variations in the $MnCl_6^{4-}$ complex along the series is noteworthy. In particular, the influence of R upon the excitation spectra is clearly illustrated in Fig. 3 through the redshifts experienced by the first $^4T_{1g}$ and $^4T_{2g}$ bands on passing from $CsSrCl_3$ to $KMgCl_3$. According to the Tanabe–Sugano diagram for d^5 ions [23], these shifts clearly reflect an increase of $10Dq$ which must be associated with a reduction of R. This effect is also evidenced by looking at the energy separation displayed by the $10Dq$-independent $^4A_{1g}$, ^4E_g (G) bands and the $10Dq$-dependent $^4T_{2g}$(G) band. Suitable values of R have been obtained from the excitation spectra by assuming that $10Dq$ is proportional to R^{-5}. Apart from theoretical considerations, this assumption is justified by the experimental findings in different octahedral transition metal complexes such as MnF_6^{4-} in $ABF_3:Mn^{2+}$ [8, 9, 22] and by hydrostatic pressure experiments performed by Drickamer *et al.* [24] on Al_2O_3 doped with Ni, V, Ti and Cr. Table 1 lists the R values for the $ABCl_3:Mn^{2+}$ series calculated from the equation:

$$10Dq = 54.8R^{-5} \quad \text{(units in } cm^{-1} \text{ and Å)}. \qquad (2)$$

This equation was derived using the structural and spectroscopic data of an NH_4MnCl_3 crystal as a standard ($10Dq = 5620\ cm^{-1}$). Table 1 also includes

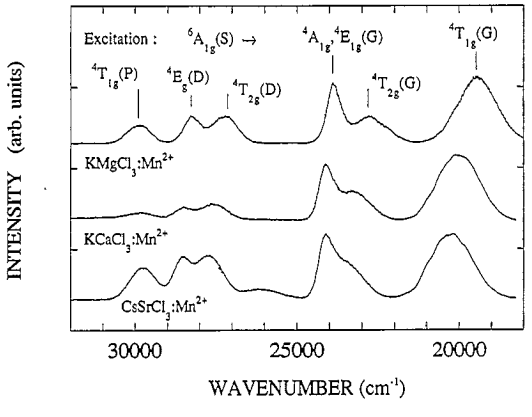

Fig. 3. Room temperature excitation spectra of $KMgCl_3:Mn^{2+}$, $KCaCl_3:Mn^{2+}$ and $CsSrCl_3:Mn^{2+}$ single crystals. Luminescence was detected at 600 nm. Band labelling is written in O_h notation.

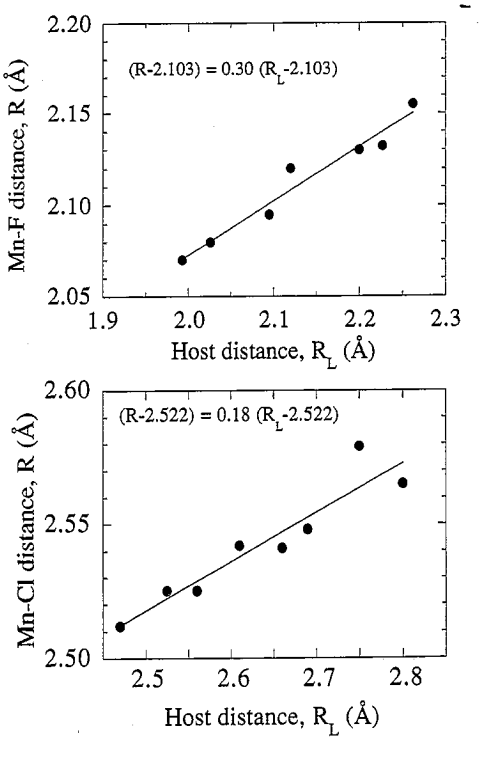

Fig. 4. Mn–ligand distance vs host distance plots for the $ABCl_3:Mn^{2+}$ (present work) and $ABF_3:Mn^{2+}$ [22] series. Straight lines and equations correspond to the linear least squares fits.

the room temperature crystallographic data for the $ABCl_3$ crystals from which we have obtained the mean B–Cl distance, R_L, through the equation,

$$R_L = \frac{1}{2}\left(\frac{V}{Z}\right)^{1/3}. \quad (3)$$

V and Z are the cell volume and the number of molecules per cell, respectively. Note that R_L does not necessarily coincide with the actual B–Cl distance unless the crystal is cubic. In other cases such as $KMgCl_3$, R is equal to or smaller than the B–Cl distance.

It must be pointed out that the present estimates give R values for $KMgCl_3$ and $RbCaCl_3$ which are equal within the experimental accuracy to those measured by EXAFS. Consequently, this result justifies the previous assumption and therefore confirms the R^{-5} dependence of $10Dq$ for this series. The fact that we experimentally observe the same R-dependence for chlorides and fluorides must not be considered as a proof of the point charge crystal field model as this cannot account for the experimental $10Dq$ values. Nevertheless, recent Xα and extended Hückel calculations performed for the MnX_6^{4-} (X = F and Cl) complexes for different bond distances confirm the behavior $10Dq = KR^{-n}$, with similar exponents for F and Cl [24]. Thus, R accuracies of $2 \cdot 10^{-3}$ Å can be obtained from this optical technique if the variation of $10Dq$ along the series is completely due to changes in the Mn–Cl distance.

The influence of the host lattice upon R for both the $MnCl_6^{4-}$ and MnF_6^{4-} complexes is illustrated in Fig. 4. The MnF_6^{4-} data are taken from Ref. [22]. As regards these variations, two important facts must be emphasized: (1) R is different from the host lattice value R_L in every case and the variation of R along the series is significantly smaller than ΔR_L, the variation of R_L. For perovskites, R lies between R_L and the Mn–ligand distance in the pure manganese crystals. (2) When Mn^{2+} is introduced into the crystal, a ligand relaxation around the Mn takes place. This relaxation, defined by the parameter $\delta R = R_L - R$, is much stronger for chlorides due to the more covalent character of the Mn–Cl bonds. In fact, the variation of R over the two series, shown in Fig. 4, can be described by the linear equations $\Delta R = R - 2.103 = 0.30\ (R_L - 2.103)$ and $\Delta R = R - 2.522 = 0.18\ (R_L - 2.522)$ for fluorides and chlorides, respectively, thus showing that local relaxations in chlorides are almost twice as large as in fluorides. On the other hand, the sums of ionic radii estimated from these curves, 2.103 and 2.520 Å, respectively, are somewhat smaller than the standard values, 2.13 and 2.56 Å, but are very similar to the Mn–X distances found in $KMnF_3$ and NH_4MnCl_3, respectively.

Finally, it should be pointed out that the present procedure for estimating bond distances from optical data cannot be applied to low symmetry crystals like $[(CH_3)_4N]MnCl_3$(TMMC) or Rb_2MnCl_4. This is because the corresponding excitation (or absorption) spectra show an energy splitting of the absorption bands resulting from the low symmetry ligand field and therefore the *effective* $10Dq$ parameters derived from such spectra do not necessarily obey eqn (2). Investigations along this line are presently in progress.

4. CONCLUSIONS

The Mn–Cl distances have been determined by two independent spectroscopies in the $ABCl_3:Mn^{2+}$ chloroperovskite family. Good agreement has been found between distances obtained by EXAFS and optical excitation spectroscopy. A salient feature of this work is the accuracy of the optical spectroscopy for estimating local distances in metal doped systems ($\Delta R \sim 0.002$ Å). Furthermore, the higher sensitivity of the optical techniques with respect to EXAFS can be exploited to measure local distances in materials of technological interest doped with low concentrations of metal impurities. Nevertheless, the present method must be applied to high-symmetry systems since the $10Dq$ values derived from the optical spectra can significantly deviate from the actual $10Dq$ values in low-symmetry systems. In addition, the use of optical techniques for measuring local distances necessarily requires previous correlation studies with EXAFS in order to get reliable standards.

Concerning $ABCl_3:Mn^{2+}$, it must be observed that the variation of the Mn–Cl distance over the crystal series is proportional to the variation of the host lattice distance, but in no case do these distances coincide with each other. A relaxation of the Cl ligands takes place around the Mn, with a value proportional to $R_L - 2.522$ (Å), where R_L is the host distance and 2.522 Å is close to the Mn–Cl distance in pure NH_4MnCl_3 perovskite. Though these results are quite similar to those found for the isomorphous $ABF_3:Mn^{2+}$ series, a stronger lattice relaxation is observed in the chlorides. This fact is associated with the more covalent character of the Mn–Cl bond.

Acknowledgements—We thank Dr A. Mickalowitz for kindly providing us with the software program package for EXAFS analysis and Dr D. Parent for technical assistance. We also acknowledge financial support from the Swiss National Science Foundation and the CYCIT (Project No. PB92-0505).

REFERENCES

1. Catlow C. R. A., Chadwick A. V., Greaves G. N. and Moroney L. M., *Nature (Lond.)* **312,** 601 (1984).
2. Vernon S. P. and Stearns M. B., *Phys. Rev. B* **46,** 6968 (1984).
3. Barkyoumb J. H. and Mansour A. N., *Phys. Rev. B* **46,** 8768 (1992).
4. Leblé A., Thèse d'Etat, Université du Maine, Le Mans (1982).
5. Jacobi Y. and Stern E. A., *Ferroelectrics* **125,** 263 (1992).
6. Zaldo C., Prieto C., Dexpert H. and Fessler P., *J. Phys.: Condens. Matter* **3,** 4135 (1991).
7. Barriuso M. T. and Moreno M., *Phys. Rev. B* **29,** 3623 (1984).
8. Rodríguez F. and Moreno M., *J. Chem. Phys.* **84,** 692 (1986).
9. Rodríguez F., Moreno M., Tressaud A. and Chaminade J. P., *Cryst. Latt. Def. Amorph. Mater.* **16,** 221 (1987).
10. Fujii Y., Hoshino S., Yamada Y. and Shirane G., *Phys. Rev. B* **9,** 4549 (1974).
11. Vaills Y., Buzaré J. Y., Gibaud A. and Launary C., *Solid State Commun.* **60,** 139 (1986).
12. Brynestad J., Yakel H. L. and Smith G. P., *J. Chem. Phys.* **45,** 4652 (1966).
13. *International Tables of X-ray Crystallography*, Vol. IV. The Kynoch Press, Birmingham (1974).
14. Marco de Lucas M. C., Rodríguez F., Güdel H. U. and Furer N., *J. Luminesc.* **60/61,** 581 (1994).
15. Michalowicz A., in *EXAFS pur le MAC, Logiciels por la Chimie.* Societé Francaise de Chimie, Paris (1991).
16. Michalowicz A., Verdaguer M., Mathey Y. and Clement R., *Topics in Current Chemistry* **145,** 107 (1988).
17. Sayers D. E., Stern E. A. and Lytle F. W., *Phys. Rev. Lett.* **27,** 1204 (1971).
18. Morosin B. and Graeber E. J., *Acta Crystallogr.* **23,** 766 (1967).
19. Agulló-Rueda F., Calleja J. M., Jaque F. and Tornero J. D., *Solid State Commun.* **60,** 331 (1986).
20. Briois V., Lequan R. M., Lequan M., Carier C., Van der Laan G., Michalowicz A. and Verdaguer M., *Chem, Mater.* **4,** 484 (1992).
21. Tichy K., Benes J., Hälg W. and Arend H., *Acta Crystallogr. B* **34,** 2970 (1978).
22. Marco de Lucas M. C., Rodríguez F. and Moreno M., *J. Phys.: Condens. Matter* **5,** 1437 (1993).
23. Griffith J. S., in *The Theory of Transition Metal Ions.* Cambridge University Press, Cambridge (1980).
24. Drickamer H. G. and Franck C. W., in *Electronic Transitions and the High Pressure Chemistry and Physics of Solids.* Chapman and Hall, London (1973).
25. Seifert H. J. and Uebach J., *J. Solid State Chem.* **59,** 86 (1985).
26. Midorikawa M., Miwa S. and Ishibashi Y., *Mater. Res. Bull.* **14,** 987 (1979).
27. McCurdie H. F., De Groot J., Morris M. and Swanson H. E., *J. Res. Natl Bur. Stand.* **73A,** 621 (1969).
28. Plesko S., Kind R. and Roos J., *J. Phys. Soc. Jpn* **45,** 553 (1978).
29. Seifert H. J., Fink H., Thiel G. and Uebach J., *Z. Anorg. Allg. Chem.* **520,** 151 (1985).
30. Midorikawa M., Ishibashi Y. and Takagi Y., *J. Phys. Soc. Jpn* **46,** 1240 (1979).
31. Fink V. H. and Seifert H. J., *Z. Anorg. Allg. Chem.* **466,** 87 (1980).
32. Midorikawa M., Ishibashi Y. and Takagi Y., *J. Phys. Soc. Jpn* **41,** 2001 (1976).
33. Alexandrov K. S., Anistratov A. T., Melnikova S. V., Zinenko V. I., Shabanova L. A. and Beznosikov B. V., *Ferroelectrics* **20,** 305 (1978).